



Research article

Analysis of the dynamics of new models of nonlinear systems with state variable damping and elastic coefficients

R.F. Fonkou^{a,b,c,*}, Patrick Louodop^b, P.K. Talla^c, P. Wofo^a^a Laboratory of Modeling and Simulation in Engineering, Biomimetics and Prototypes, Faculty of Science and TWAS Research Unit, University of Yaounde I, Box 812, Yaoundé, Cameroon^b Research Unit Condensed Matter, Electronics and Signal Processing, Université de Dschang, P.O. Box 67 Dschang, Cameroon^c UR de Mécanique et de Modélisation des Systèmes Physiques (UR-2MSP), UFR/DSST, Université de Dschang, BP 67 Dschang, Cameroon

ARTICLE INFO

Keywords:

Keywords nonlinear systems
Elastic coefficients
Limit cycle
Artificial pacemaker
State variable damping
Regular and chaotic behaviors
Microcontroller technology

ABSTRACT

This paper, is an analysis of the dynamics of new models of nonlinear systems in which the state damping variables with elastic coefficients, given by functions $c \cos(px)$, $c \sin(px)$, $c \cos(px)$ and $c \sin(px)$ are investigated in their autonomous and excited states. They exhibit periodic regions of stability and instability in their autonomous states and a rich dynamic behavior. The analysis of limit cycles shows the presence of isolated curves around the origin (0.0), which explains the presence of periodic solutions (limit cycles). The dynamics obtained allows to describe qualitatively the cardiac activity (artificial pacemaker). A chaos analysis shows the appearance of regular and chaotic behaviors. These studies allowed us to show the effect of the damping of the state variable and the elastic coefficients on the dynamics of these models. The presence of analog functions makes the experimental study complex. An implementation based on microcontroller simulation technology has been proposed. The microcontroller results are consistent with the numerical results.

1. Introduction

Owing to their broad importance in many fields and their numerous engineering applications, nonlinear oscillators have recently attracted the attention of a large number of researchers due to their extremely rich dynamics (Joshi, 2021; Dashkovskiy and Pavlichkov, 2020; Ahmed et al., 2017; Cheng and Zhan, 2020; Kudryashov, 2018; Tang et al., 2020; Dashkovskiy and Pavlichkov, 2020; Fonkou et al., 2022; Han et al., 2019; Ramirez et al., 2020; FitzHugh, 1961; Rahman et al., 2021a,b,c,d). Their fields of application are between others: seismology, communication and neurophysiology (Rahman et al., 2021a,b,c,d; Lucero and Schoentgen, 2013; Rowat and Selverston, 1993; Balachandran and Kandiban, 2009). These oscillators exhibit rich dynamics among which limit cycle oscillations of sinusoidal and relaxation nature, since one of their important characteristic is their capacity to present limit cycle behaviors which is an important criterion in the characterization of the artificial pacemaker (Steeb, 1977; Hochstadt and Stephan, 1967; D'Heedene, 1996; Steeb and Kunick, 1987; Steeb et al., 1983). When subjected to an external periodic excitation, numerical studies and singular point analysis have revealed chaotic behaviors,

allowing the analysis of phenomena such as control and cardiac activity with numerous technological applications. (Steeb and Kunick, 1982; Steeb and Kunick, 1983; Forger, 1999; Enrique et al., 2020; Rahman et al., 2019; Kai and Tomita, 1979; Rahman et al., 2021a,b,c,d; Van der Pol and Van der Mark, 1926; Van der Pol and Van der Mark, 1928; Alhasnawi et al., 2021).

The Van der Pol oscillator is one of these systems, it is nonlinear and its differential equation is the second order. It is a self-sustained oscillator because it maintains its oscillations by itself. Under certain conditions, it also exhibits the very rich dynamical behaviors (Van der Pol and Van der Mark, 1928; Alhasnawi et al., 2021; Chedjou et al., 1997; Makouo and Wofo, 2017; Han et al., 2018; Simo and Wofo, 2012; Bao et al., 2018; Jasim et al., 2020; Han and Bi, 2012; Ma et al., 2021; Grudzinski and Zebrowski, 2004; Magnitskii and Sidorov, 2004). The refs. (Van der Pol and Van der Mark, 1926; Van der Pol and Van der Mark, 1928) have shown that the qualitative characteristics of the heart action potential are closely related to the dynamic response of the classical Van der Pol oscillator (VdP), because it is the starting point for modeling heartbeats.

* Corresponding author at: Research Unit Condensed Matter, Electronics and Signal Processing, Université de Dschang, P.O. Box 67 Dschang, Cameroon.

E-mail address: fonkourodriague99@yahoo.com (R.F. Fonkou).

URL: <http://www.lamsebp.org> (R.F. Fonkou).

<https://doi.org/10.1016/j.heliyon.2022.e10112>

Received 19 March 2022; Received in revised form 8 May 2022; Accepted 25 July 2022

In the work of Refs. (Steeb and Kunick, 1987; Steeb et al., 1983), the authors study the dynamic behavior of anharmonic systems with limit cycles in which the potentials are only dependent variables. The models used are modifications of the Van der Pol oscillator, the appearance of chaotic dynamics and limit cycle dynamics is due solely to the effect of potentials and the damping coefficient.

In the present work, an analysis of the dynamics of four new models of nonlinear systems under external periodic disturbance is proposed: analytical study and experimental simulation by microcontroller. These models have state variable damping and elastic coefficients. They are described by equations (1) and (2).

However, periodic sine or cosine function of system variable may introduce some coexisting attractors based on offset boosting and therefore self-reproducing chaotic system may be devised.

Faced with this, the following question was asked: how can sinusoidal functions show monotonic solutions of limit cycles and the onset of chaotic dynamics under external excitation? To answer this question, the present work has been organized as follows: Section 2 presents a description of the models used. Section 3 presents an analysis of their dynamics in their autonomous states. Section 4 is devoted to the study of the systems in the excited state. Section 5 shows the results through the practical implementation using an Arduino Uno board. Section 6 ends with the conclusion.

2. Description of the models

Four new nonlinear oscillator models in which the variables have been substituted by the terms with state variable damping and elastic coefficients given by functions $c \cos(px)$, $c \sin(px)$, $c \cos(p\dot{x})$ and $c \sin(p\dot{x})$ are used. Eq. (1) and Eq. (2) present their dynamics

$$\ddot{x} + (a - f(x))\dot{x} + bx = 0 \tag{1}$$

$$\ddot{x} + a\dot{x} + (b - f(\dot{x}))x = 0 \tag{2}$$

With

$$f(x) = \begin{cases} c \cos(px) \\ c \sin(px) \end{cases} \quad \text{and} \quad f(\dot{x}) = \begin{cases} c \cos(p\dot{x}) \\ c \sin(p\dot{x}) \end{cases}$$

With a, b, c , and p , the characteristic parameters of systems. To maintain the self-oscillating character of the systems, these coefficients must be positive. For an expansion of the functions $f(x)$ and $f(\dot{x})$ up to the order two, the so-called Van der Pol equation is obtained, which is important for triode oscillators necessary for the characterization of the heart (Van der Pol and Van der Mark, 1928). Qualitatively, the quantity $\frac{a}{c}$ represents the friction, if this one is very ($c \gg a$), one obtains an autonomous oscillatory character and the fixed point unstable tends with the complex eigenvalues of the Jacobean matrix towards a repulsive focus. On the other hand, if it is very strong ($a \gg c$) the oscillatory character is not autonomous and the fixed point stable tends towards an attractive focus with the complex eigenvalues of the Jacobean matrix. Thus $\frac{a}{c}$ influence on the more or less sinusoidal character of these systems.

Quantitatively, the frequency character of the system is linked to the quantity b . Thus, when b increases, the frequency of the oscillations increases and their amplitude decreases. On the other hand, the decrease in b leads to a decrease in the frequency of the oscillations but an increase in their amplitude. Being the natural frequency of the systems, b is chosen so that the systems evolve with a frequency of $f_0 = 1$ Hz which is the mean frequency of a healthy heart (Van der Pol and Van der Mark, 1926). Where p is a constant. Using these very rich dynamics, the artificial pacemaker can be a very important application of these models.

3. Analysis of dynamics in their autonomous state

3.1. Analysis of stability

Equation (1) can be rewritten as follows:

$$\begin{cases} \dot{x} = y \\ \dot{y} = -(a - f(x))y - bx \end{cases} \tag{3}$$

Obtaining the equilibrium points be done by solving the system below:

$$\begin{cases} \dot{x} = 0 \\ \dot{y} = 0 \end{cases} \tag{4}$$

For $f(x) = c \cos(px)$ the resulting fixed point is $A_1(0,0)$. The Jacobean matrix obtained from this point $J_1 = \begin{bmatrix} 0 & 1 \\ -b & -a + ac \end{bmatrix}$. By solving $Det(J_1 - \lambda I) = 0$, the resulting characteristic equation is $\lambda^2 - (ca - a)\lambda + b = 0$ and the discriminant is $\Delta_1 = (ca - a)^2 - 4b$.

However, for $f(x) = c \sin(px)$, the fixed point is given by $A_2(0,0)$. Its Jacobean matrix is $J_2 = \begin{bmatrix} 0 & 1 \\ -b & -a \end{bmatrix}$. The characteristic equation obtained by solving $Det(J_2 - \lambda I) = 0$, is $\lambda^2 + a\lambda + b = 0$ and its discriminant $\Delta_1 = a^2 - 4b$.

It can be seen that:

- For $\Delta_1 > 0$ and $\Delta_2 > 0$, A_1 unstable and A_2 is stable.
- For $\Delta_1 < 0$ and $\Delta_2 < 0$, if $c \in]a; a + 2\sqrt{b}[$, A_1 is unstable. However, if $c \in]\leftarrow; a[$, A_1 is stable. For $a \in]0; 2\sqrt{b}[$, A_2 is stable however if $a \in]\leftarrow; 0[$, A_2 is unstable.
- For $\Delta_1 = 0$ and $\Delta_2 = 0$, if $a < 0$, A_1 is unstable, if $a > 0$, A_1 is stable. However, A_2 is stable.

By considering the Eq. (2), it can still be written by:

$$\begin{cases} \dot{x} = y \\ \dot{y} = -ay - (b - f(y))x \end{cases} \tag{5}$$

From equation (4), we obtain for $f(\dot{x}) = c \cos(p\dot{x})$, the fixed point $A_3(0,0)$. Its Jacobean matrix is $J_3 = \begin{bmatrix} 0 & 1 \\ c - b & -a \end{bmatrix}$. By solving $Det(J_3 - \lambda I) = 0$, its characteristic equation gives $\lambda^2 + a\lambda + b - c = 0$ and its discriminant $\Delta_3 = a^2 + 4(b - c)$.

However, for $f(\dot{x}) = c \sin(p\dot{x})$, the fixed point is $A_4(0,0)$. The Jacobean matrix is $J_4 = \begin{bmatrix} 0 & 1 \\ -b & -a \end{bmatrix}$. The characteristic equation obtained by solving $Det(J_4 - \lambda I) = 0$ is given by $\lambda^2 + a\lambda + b = 0$ and the discriminant by $\Delta_1 = a^2 - 4b$. $I = \begin{bmatrix} 0 & 1 \\ 1 & 0 \end{bmatrix}$ is the identity matrix.

Thus we have:

- For $\Delta_3 \geq 0$ and $\Delta_4 \geq 0$, A_3 and A_4 are stable.
- For $\Delta_3 < 0$ and $\Delta_4 < 0$, if $a \in]0; 2\sqrt{b - c}[$, A_3 is stable. However, if $a \in]\leftarrow; 0[$, A_3 is unstable. For $a \in]0; 2\sqrt{b}[$, A_4 is stable and unstable if $a \in]\leftarrow; 0[$.

Be it Eq. (1) where Eq. (2) we find that when, ($c < a$) the equilibrium point is stable and the models converge. On the other hand when ($a < c$), the equilibrium point is unstable and the models diverge.

The only critical point being the origin (zero coordinates), a solution of period one exists. In the (x, y) -plane, this solution can describe limit cycle dynamics

3.2. Analysis of the dynamics of limit cycles

Recent studies on the nature of integral curves have shown the presence of singular points in systems of differential equations (Chaté, 1994; Bendixson, 1901). Generally, they are observed in conservative systems. However, for some non-conservative systems, closed trajectories

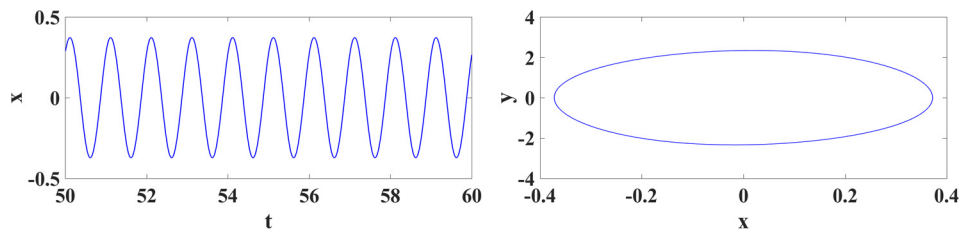


Fig. 1. Time series and phase portrait obtained from Eq. (1) with $a = 0.5$, $b = 39.4384$, $p = 5$, $x(0) = 0.01$, and $dx/dt(0) = 0.04$.

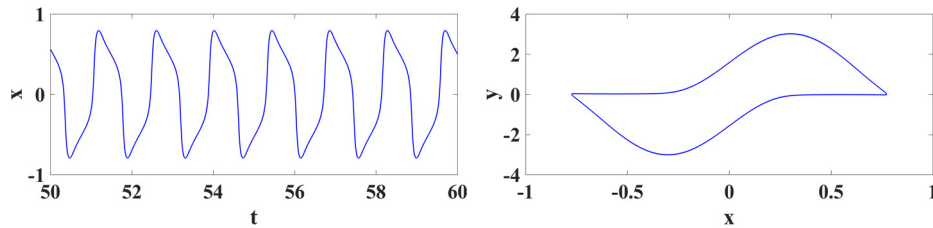


Fig. 2. Time plots and phase portrait obtained from Eq. (1) with $a = 0.5$, $b = 39.4384$, $p = 5$, $x(0) = 0.01$, and $dx/dt(0) = 0.04$.

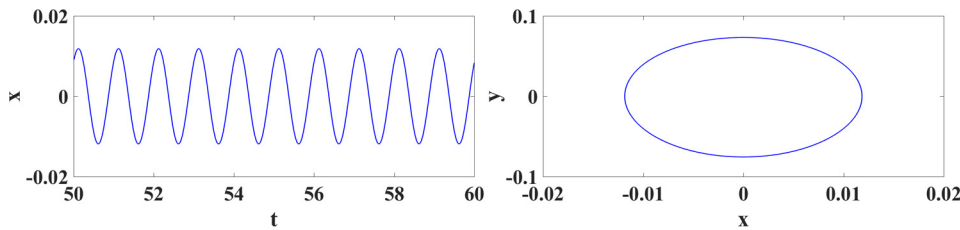


Fig. 3. Time plots and phase portrait obtained from Eq. (1) with $a = 0.001$, $b = 39.4384$, $c = 5$, $p = 5$, $x(0) = 0.01$, and $dx/dt(0) = 0.04$.

or limit cycles could be approached. Eqs. (6) and (7) describe the dynamics of a nonlinear system of order 2

$$\frac{dx}{dt} = X(x, y) \tag{6}$$

And

$$\frac{dy}{dt} = Y(x, y) \tag{7}$$

Then a limit cycle is necessarily formed in a domain whose limits are respectively the innermost and most external circles of radii R_{min} and R_{max} which touch the contact curve (Hayashi, 1964).

By considering the models (3) and (5), since the origin is an only singular point, a family of concentric circles around this origin is considered, that is to say:

$$x^2 + y^2 = const \tag{8}$$

In this paragraph, it will be demonstrated that the models described by systems (3) and (5) exhibit limit cycle oscillations under origin (0, 0).

By considering Eq. (1), for $f(x) = c \cos(px)$, starting from the given Eq. (8), we obtain:

$$\frac{dy}{dx} = \frac{x}{y} \tag{9}$$

When the polar coordinates given by Eq. (10) are introduced in Eq. (9), and apart from $r = 0$, the expressions of the radii R_{min} and R_{max} are presented in Eq. (11):

$$\begin{cases} x = r \cos \theta \\ y = r \sin \theta \end{cases} \tag{10}$$

$$\begin{cases} R_{min} = \sqrt{\frac{4(b-1)+4(a-c)}{cp^4}} \\ R_{max} = \sqrt{\frac{4(b-1)+4(c-a)}{cp^4}} \end{cases} \tag{11}$$

Still in considering Eq. (1), but this time with $f(x) = c \sin(px)$, the expressions of the radii R_{min} and R_{max} are given by:

$$\begin{cases} R_{min} = \frac{4a}{cp^2} \\ R_{max} = \frac{b-1}{cp^2} \end{cases} \tag{12}$$

When the dynamics of system are described by Eq. (2) with $f(x) = c \cos(px)$, by substituting Eq. (10) in Eq. (9) and apart from $r = 0$, the expressions of the radii R_{min} and R_{max} are given by:

$$\begin{cases} R_{min} = \sqrt{\frac{2b-4a-2(1+c)}{cp^4}} \\ R_{max} = \sqrt{\frac{2b+4a-2(1+c)}{cp^4}} \end{cases} \tag{13}$$

Still by taking Eq. (2) with $f(x) = c \sin(px)$, the expressions of the radii R_{min} and R_{max} are given by:

$$\begin{cases} R_{min} = \frac{4a}{cp^2} \\ R_{max} = \frac{4(b-1)}{cp^2} \end{cases} \tag{14}$$

Consequently from expressions given in (11), (12), (13), and (14), a ring domain centered at the origin exists and contains all possible limit cycles; these boundaries are the radii R_{min} and R_{max} . They represent the boundaries of the innermost and outermost circles, respectively, that touch the contact curve. These expressions show that if a limit cycle occurs around the origin, it must necessarily be in a ring domain whose center is at the singular point.

In Figs. 1, 2, 3, 4, and 5, the temporal traces and phase portraits have been plotted for the initial conditions $x(t = 0)$ and $y(t = 0)$. This allows us to observe that these systems are nonlinear and self-excited and show limit cycle behaviors of sinusoidal and relaxation nature. The limit cycles are almost isolated curves so the trajectories converge around the origin.

The limit cycles obtained from Eq. (1) (case of $f(x) = c \cos(px)$) are presented by figure.

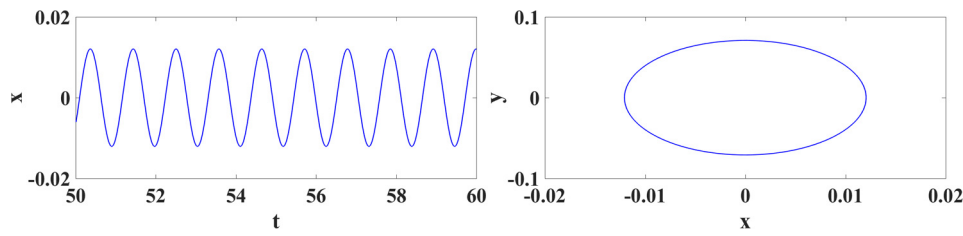


Fig. 4. Time plots and phase portrait obtained from Eq. (2) with $a = 0.001$, $b = 39.4384$, $c = 5$, $p = 5$, $x(0) = 0.01$, and $dx/dt(0) = 0.04$.

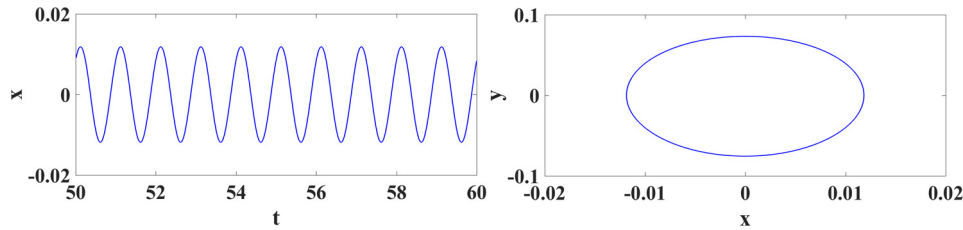


Fig. 5. Time plots and phase portrait obtained from Eq. (2) with $a = 0.001$, $b = 39.4384$, $c = 5$, $p = 5$, $x(0) = 0.01$, and $dx/dt(0) = 0.04$.

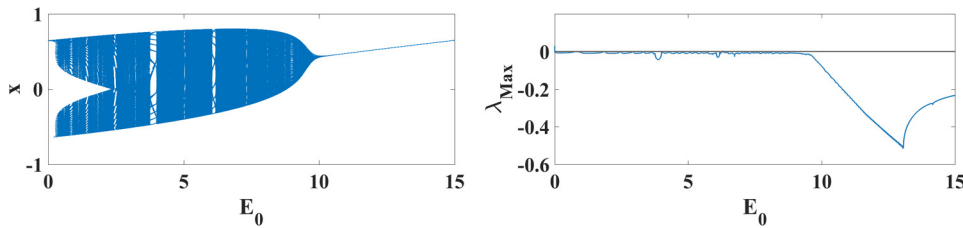


Fig. 6. Bifurcation tree and Lyapunov exponent obtained when Eq. (1) is excited (case of $f(x) = c \cos(px)$), with $\omega = 4.8 \text{ rad.s}^{-1}$, $a = 0.5$, $b = 0.25$, $c = 2$ and $p = 5$.

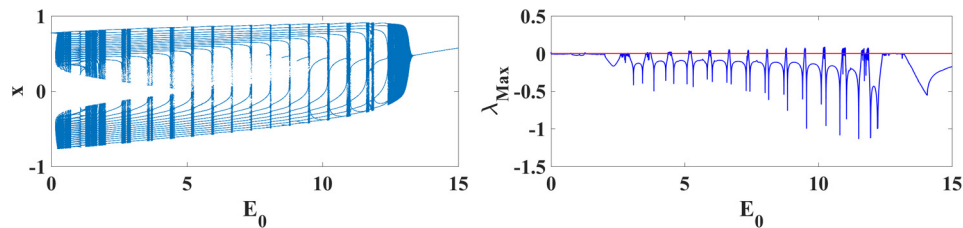


Fig. 7. Bifurcation tree and Lyapunov exponent obtained when Eq. (1) is excited (case of $f(x) = c \cos(px)$), with $\omega = 4.8 \text{ rad.s}^{-1}$, $a = 0.5$, $b = 0.25$, $c = 8$ and $p = 5$.

For $c = 2$, the temporal trace and phase portrait are given in Fig. 1.

On the other hand, for $c = 8$, we have Fig. 2.

Still by considering Eq. (1) (case of $f(x) = c \sin(px)$), the time serie and the phase portrait are given in Fig. 3.

By considering the Eq. (2) (case of $f(\dot{x}) = c \cos(p\dot{x})$), the limit cycles are given in Fig. 4.

When we consider Eq. (2) (case of $f(\dot{x}) = c \sin(p\dot{x})$), the time plot and phase portrait are given in Fig. 5.

It can be seen in Figs. 1, 2, 3, 4, and 5 that the models used are nonlinear and self-excited and exhibit limit cycle dynamics of sinusoidal and relaxation nature qualitatively comparable with those exhibited by artificial pacemakers (Van der Pol and Van der Mark, 1928). In addition, the sinusoidal oscillations evolve with a frequency of 1 Hz for $b = \omega_0^2$ where $\omega_0 = 2\pi f_0$ and $f_0 = 1 \text{ Hz}$.

4. Analysis of dynamics in their excited state

4.1. Chaos analysis

In the anharmonic systems with limit cycles, it has been shown that the variation of their parameters as well as those of the external force can lead to chaotic behaviors. The Refs. (Steeb and Kunick, 1987; Steeb et al., 1983) have demonstrated the influence of potentials and damped

coefficients on the appearance of chaotic dynamics in nonlinear systems. In this study, our objective is to see the effect of state variable damping and elastic coefficients on the appearance of chaotic dynamics in nonlinear systems under the effect of an external excitation of sinusoidal nature $E_0 \sin(\omega t)$. This is done by plotting the bifurcation curves each associated with its maximum Lyapunov exponent with the amplitude of the external excitation E_0 as parameter. These curves (bifurcation and maximum Lyapunov exponent) are presented in Figs. 6, 7, 8, and 9. On these figures, we observed the presence of chaotic and multiperiodic dynamics. However, for small values of the parameter E_0 , the Lyapunov exponent tends towards 0. This behavior reflects the presence of quasiperiodic dynamics. A few are shown in Fig. 6. In Fig. 11 it only about the presentation of some phase portraits illustrating the chaotic states.

When Eq. (1) is excited (case of $f(x) = c \cos(px)$), the bifurcation trees and maximal Lyapunov exponents are given in Figs. 6 and 7.

When $c = 2$, the information given by Fig. 6 are: a period-2T orbit $E_0 \leq 0.2V$ is obtained, this behavior disappears and gives way to the quasiperiodic behavior for $0.2V \leq E_0 < 3.75V$. A second orbit of period-13T appears for $3.75V \leq E_0 < 4.0V$, then disappears to give a quasiperiodic orbit for $4.0V \leq E_0 < 6.0V$. For $6.0V \leq E_0 < 6.2V$, a new orbit of period-11T is observed, the latter disappears and gives a quasiperiodic

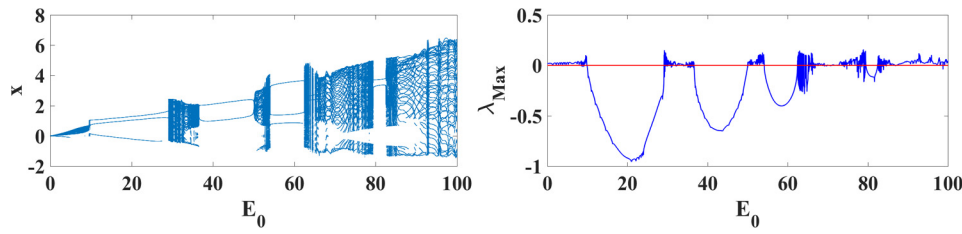


Fig. 8. Bifurcation tree and Lyapunov exponent obtained when Eq. (1) is excited (case of $f(x) = c \sin(px)$) with $\omega = 4.8 \text{rad.s}^{-1}$, $a = 0.001$, $b = 50.25$, $c = 5$, and $p = 5$.

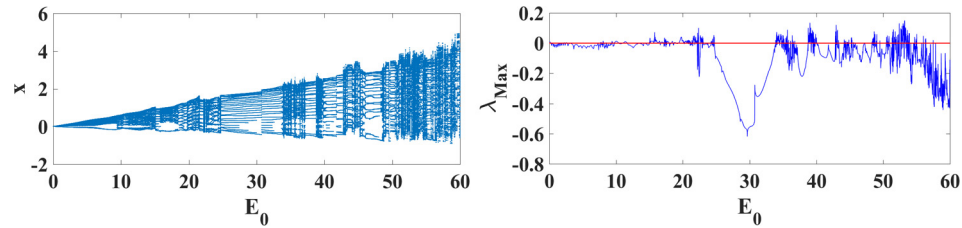


Fig. 9. Bifurcation tree and Lyapunov exponent obtained when Eq. (2) is excited (case of $f(x) = c \cos(px)$) with $\omega = 4.8 \text{rad.s}^{-1}$, $a = 0.001$, $b = 50.25$, $c = 5$, and $p = 5$.

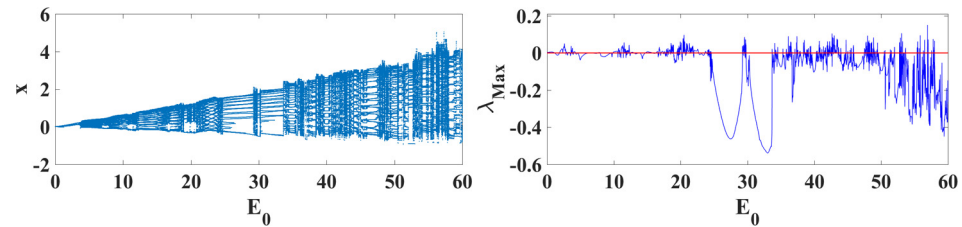


Fig. 10. Bifurcation tree and Lyapunov exponent obtained when Eq. (2) is excited (case of $f(x) = c \sin(px)$) with $\omega = 4.8 \text{rad.s}^{-1}$, $a = 0.001$, $b = 50.25$, $c = 5$, and $p = 5$.

behavior for $6.2V \leq E_0 < 9.0V$. When $E_0 \leq 9.0V$, the orbit of period-1T settles.

On the other hand, when $c = 8$, on the Fig. 7, an orbit of period-1T appears for $0.0V \leq E_0 < 0.25V$ then disappears and gives way to the quasiperiodic orbit for $0.25V \leq E_0 < 1.475V$. For $E_0 \in [1.475; 1.625[V$ the first orbit of period-34T appears. When the value of E_0 goes from $1.625V$ to $2.5V$, a second quasiperiodic orbit appears and disappears, giving way to the period-32T orbit for $2.5V \leq E_0 < 2.625V$. For $2.625V \leq E_0 < 3.0V$, quasiperiodic orbits appear, a second orbit of period-30T appears for $3.0V \leq E_0 < 3.5V$. This orbit disappears and the first chaotic behavior appears for $3.5V \leq E_0 < 3.776V$. This first chaotic behavior is replaced by a second orbit of period-27T when the value of E_0 increases from $3.776V$ to $4.385V$. Then a second chaotic orbit appears for $4.385V \leq E_0 < 4.559V$. Subsequently, the alternations between periodic and chaotic orbits are observed. For $E_0 \in [4.559; 5.172[V$ an orbit of period 25T is observed. When $5.172V \leq E_0 < 5.267V$ a third chaotic orbit is obtained. Then a new orbit of period-23T for $E_0 \in [5.267; 5.91[V$. For $5.91V \leq E_0 < 5.975V$ a fourth chaotic orbit appears. Between $5.975V$ and $6.642V$, an orbit of period-21T is also observed. A fifth chaotic orbit between $6.642V$ and $6.696V$. For $6.696V \leq E_0 < 7.319V$, a new orbit of period-19T appears. When $E_0 \in [7.319; 7.396[V$ a sixth chaotic orbit appears. Between $7.396V$ and $8.07V$ an orbit of period-17T appears. Between $8.07V$ and $8.14V$ a seventh chaotic orbit is observed. Between $8.14V$ and $8.769V$ an orbit of period-15T is obtained. For $8.769V \leq E_0 < 8.865V$ an eighth chaotic orbit appears. For $8.865V \leq E_0 < 9.46V$ an orbit of period-14T appears. Between $9.46V$ and $9.53V$, a ninth chaotic behavior is obtained. Between $9.53V$ and $10.18V$ the orbit of period-13T appears. For $10.18V \leq E_0 < 10.27V$, a tenth chaotic orbit is obtained. Between $10.27V$ and $10.89V$, an orbit of period-11T appears and between $10.89V$ and $11.02V$ an eleventh chaotic behavior is obtained. For $11.02V \leq E_0 < 11.61V$, the orbit of period-9T is observed and for $11.61V \leq E_0 < 11.88V$, a twelfth chaotic behavior. When E_0 varies between $11.88V$ and $12.4V$, there is the appearance of a period-7T

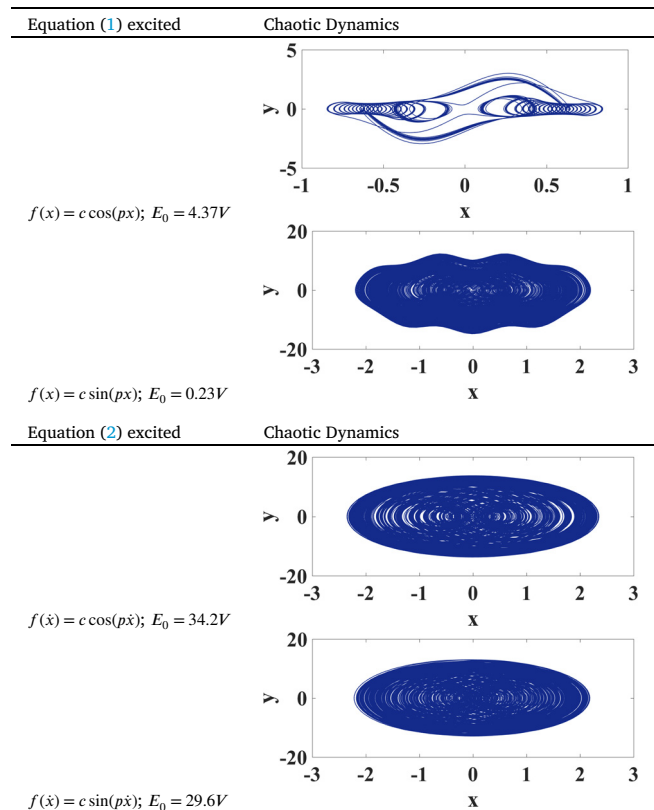


Fig. 11. Chaotic phase portraits for $x(0) = 0.01$ and $dx/dt(0) = 0.04$.

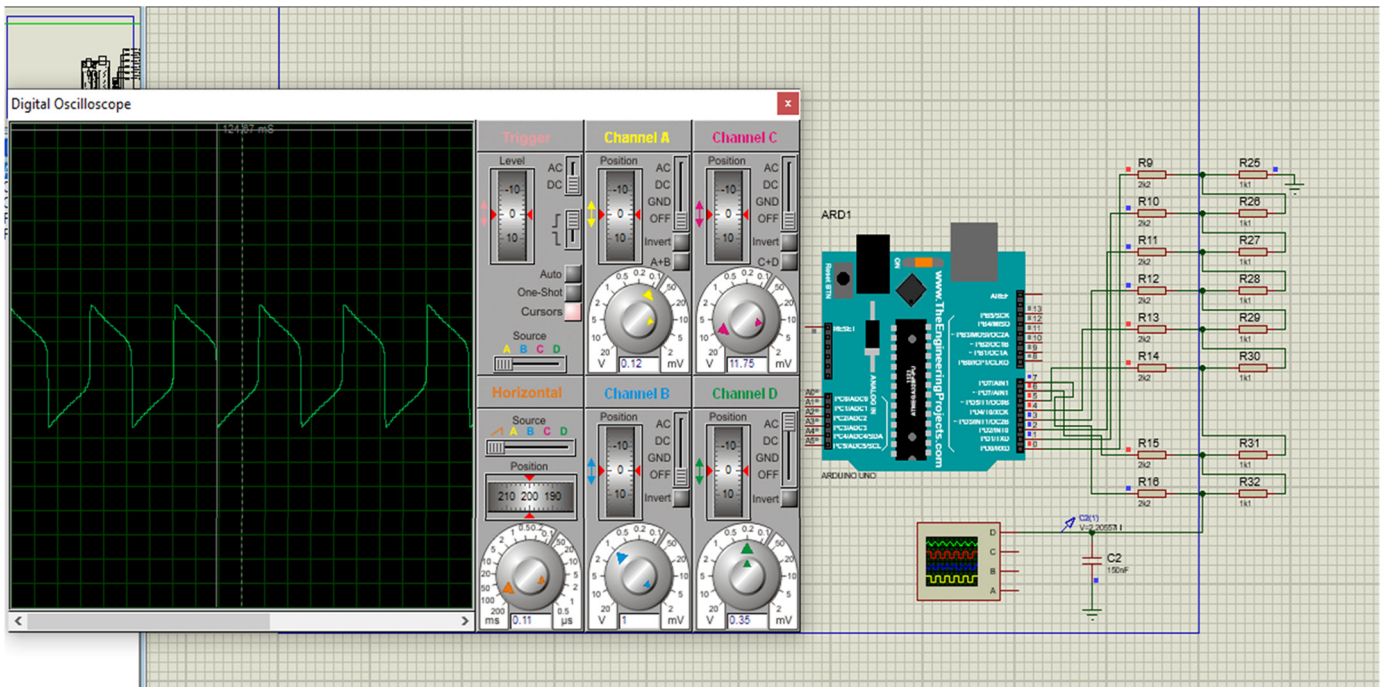


Fig. 12. Device mounted on Proteus allowing the observation of the signal on its oscilloscope.

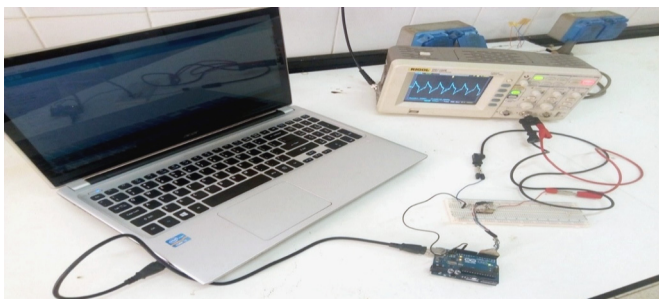


Fig. 13. Experimental device allowing the visualization of the signal.

orbit. However, between 12.4V and 13.35V, the quasiperiodic orbit reappears. From $E_0 = 13.35V$, only the orbit of period 1T evolves.

When we excite Eq. (1) (case of $f(x) = c \sin(px)$), we have in Fig. 8 the bifurcation tree and its associated maximal Lyapunov exponent.

For this case, a chaotic orbit is obtained for $0.0V \leq E_0 < 10.0V$, it then disappears and gives way to the period-3T orbit for $10.0V \leq E_0 < 28.5V$. For $E_0 \in [28.5; 36.5[V$ a new chaotic orbit appears. When the value of E_0 goes from 36.5V to 50V, a second orbit of period-2T appears, then disappears, giving way to a new chaotic orbit for $50.0V \leq E_0 < 53.5V$. For $53.5V \leq E_0 < 62.0V$, A new appearance of the period-3T orbit. A third chaotic orbit appears for $62.0V \leq E_0 < 64.5V$. This orbit disappears and the first quasiperiodic orbit appears for $64.5V \leq E_0 < 72.5V$. Then, we observe a succession between chaotic and quasiperiodic orbits for $72.5V \leq E_0 < 79.0V$. Then reappearance of the period-2T orbit for $79.0V \leq E_0 < 83.0V$. When $83.0V \leq E_0 < 100.0V$, a new succession between chaotic and quasiperiodic orbits appears.

The bifurcation curves and maximal Lyapunov exponent are given respectively in Fig. 9 for $f(x) = c \cos(px)$ and Fig. 10 for $f(x) = c \sin(px)$.

For these cases (Fig. 9 and Fig. 10), an alternation between chaotic orbits and periodic orbits is observed.

To illustrate the chaotic behaviors presented by the bifurcation curves and Lyapunov exponents of Figs. 7, 8, 9, and 10, some phase portraits are given in Fig. 11.

5. Simulation based on microcontroller technology

Microcontroller simulation is one of the simplest because it is performed using a computer in which suitable simulation software is installed. Recent work has shown that it can be used to do electronics using just a programming language (Fonkou et al., 2021a,b,c). Experimentally, it is less cumbersome and requires significant period savings for component wiring, a higher degree of integration, and lower power consumption.

A microcontroller is an integrated circuit that gathers the essential elements of a computer. Recent work has shown that microcontrollers can be used to simulate nonlinear differential equations (Fonkou et al., 2021a,b,c) by producing simple and complex electrical signals. Compared to conventional electronic systems based on separate components, they can reduce the size of the components, as well as the cost of the products. In this work, we will use an Arduino microcontroller from the ATMEGA family (Arduino Card). Its structure is shown in Fig. 12.

To produce the electrical signal described by Eq. (1) and Eq. (2), these equations are discretized. Subsequently, a simple digital code using appropriate software (here the Arduino 1.8.9) is written and loaded into the microcontroller. The signal obtained from Proteus software with its own oscilloscope is shown in Fig. 12.

To produce this signal experimentally from a real oscilloscope, the practical configuration presented in Fig. 13 is used. It consists of a computer for inserting the digital code into the microcontroller and the oscilloscope for viewing the signal delivered by the latter. The real electrical signals obtained are given in Fig. 14, Fig. 15, and Fig. 16.

For $f(x) = c \cos(px)$, we have Fig. 14.

For $f(x) = c \sin(px)$, we obtain in figure.

These curves (Fig. 14 and Fig. 15) are in agreement with those obtained respectively in the Fig. 2 and Fig. 3.

On the other hand, when we use the Eq. (2), the dynamics are given by figure.

The curves presented in the figures above (Fig. 16a and Fig. 16b) show a good agreement with those obtained numerically (Fig. 4 and Fig. 5).

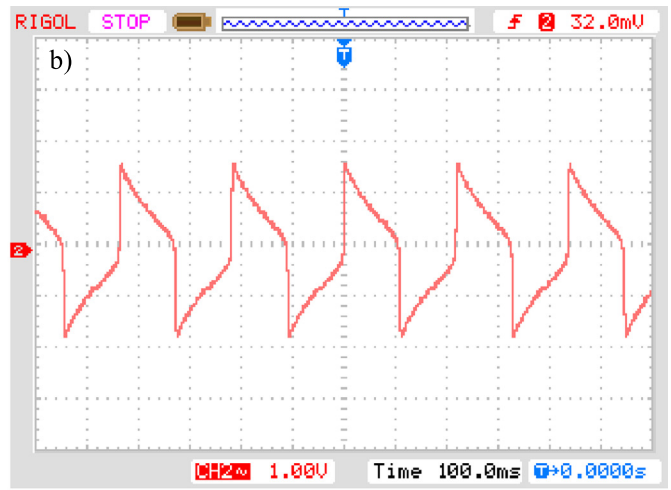
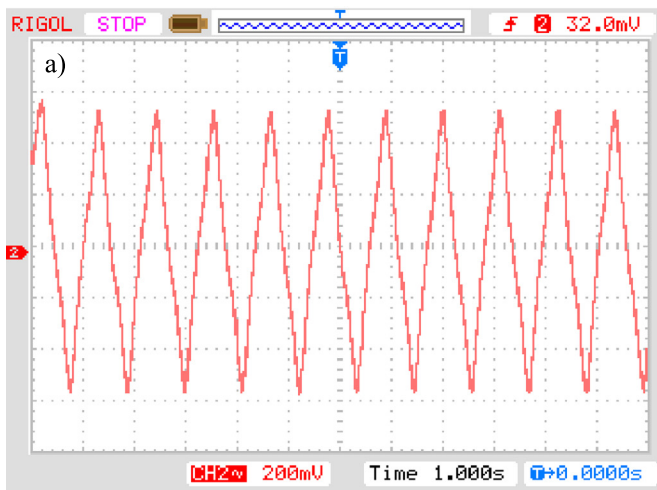


Fig. 14. Experimental results obtained from Eq. (1), with $a = 0.5, b = 0.25, c = 2, p = 5$ (Fig. 14a) and $a = 0.5, b = 0.25, c = 8, p = 5$ (Fig. 14b) for $x(0) = 0.01$ and $dx/dt(0) = 0.04$.

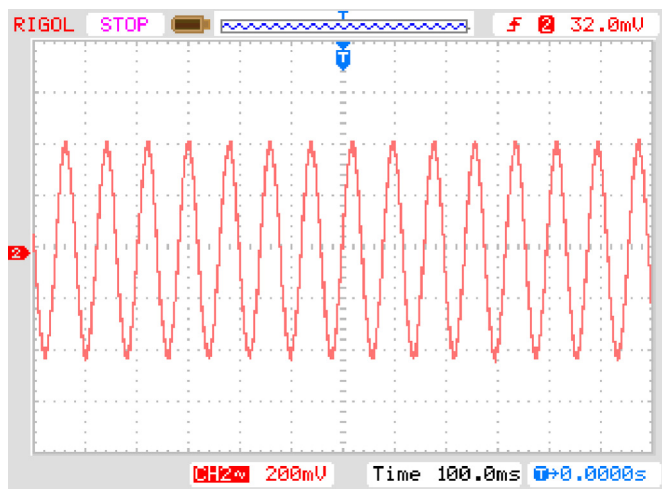


Fig. 15. Experimental results obtained from Eq. (1), with $a = 0.001, b = 50.25, c = 5, p = 5, x(0) = 0.01$, and $dx/dt(0) = 0.04$.

For the non-autonomous case, an experimental investigation similar to the autonomous case was carried out using the Runge Kutta algorithm of order 4. Two Arduino Uno boards are used practically. The first board is used to produce the electrical excitation signal $E_0 \sin(\omega t)$. The Arduino code used to produce this signal and the complete flowchart used to program this signal are given in Table 1.

The second card is used for programming the self-excited oscillator. The Arduino code and the complete flowchart used to program this oscillator are presented in Table 2.

To obtain the result, the $E_0 \sin(\omega t)$ signal produced by the first Arduino board is inserted into an input port of the second Arduino board to excite the self-excited oscillator (Eq. (1) or Eq. (2)) programmed in this second card, using an appropriate line of code.

The device cabled on Proteus is shown on Fig. 17 and its practical device is presented in Fig. 18. As shown in Figs. 19 and 20, only chaotic states have been presented.

The chaotic dynamics obtained for $f(x) = c \cos(px)$ and $f(x) = c \sin(px)$ are presented in Fig. 19. These curves show a good agreement between the experimental results and the results obtained numerically.

For $f(\dot{x}) = c \cos(p\dot{x})$ and $f(\dot{x}) = c \sin(p\dot{x})$ the chaotic dynamics obtained experimentally are presented in Fig. 20, and a good agreement between the experimental results and those obtained numerically is observed.

Table 1. The Arduino code and the complete flowchart for programming the $E_0 \sin(\omega t)$ signal

The Arduino code used to produce the signal $E_0 \sin(\omega t)$	The complete flowchart used to program the signal $E_0 \sin(\omega t)$
<pre>// constants float ts=(float)0.00016; float E0=(float)4.37; float w=(float)4.8; float t =(float)0.0; // variables float E0, ts; void setup () { pinMode (0, OUTPUT); pinMode (1, OUTPUT); pinMode (2, OUTPUT); pinMode (3, OUTPUT); pinMode (4, OUTPUT); pinMode (5, OUTPUT); pinMode (6, OUTPUT); pinMode (7, OUTPUT); } void loop() { t=t+ts; E=E0*sin(w*t); PORTD =(E-20)*45.5; t = t; }</pre>	<pre>graph TD A[Declaration of constants] --> B[Declaration of Variables] B --> C[Initialization of the Arduino Card] C --> D[Start of the Loop] D --> E[Main Program] E --> F[End of the Loop]</pre>

6. Conclusion

This work was devoted to the study of four new models of nonlinear systems with state variables damping and elastic coefficients defined by functions $c \cos(px), c \sin(px), c \cos(p\dot{x}),$ and $c \sin(p\dot{x})$. The study of limit cycles has shown that these systems, to some degree of approximation, can describe the electrical activity of the heart. The study of their dynamics in their autonomous and non-autonomous states has shown that the values of the coefficients influence the nature of the stability/instability of these systems. The production of real electrical signals by discretizing differential equations and writing digital codes in the microcontroller show that the latter can be used for the design of nonlinear oscillator models. In doing so, it appeared that when these nonlinear

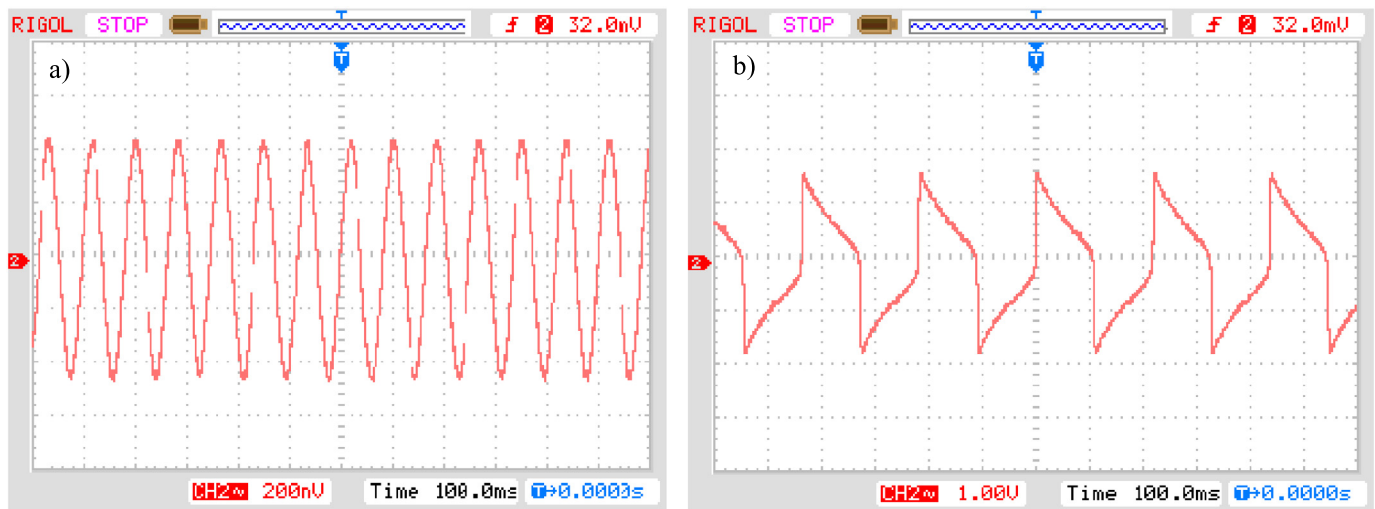


Fig. 16. Experimental results obtained from Eq. (2) (Fig. 16a: case of $f(\dot{x}) = c \cos(p\dot{x})$) and (Fig. 16b: case of $f(\dot{x}) = c \sin(p\dot{x})$) with $a = 0.001$, $b = 50.25$, $c = 5$, $p = 5$, $x(0) = 0.01$, and $dx/dt(0) = 0.04$.

systems are subjected to external and periodic sinusoidal excitation, they presented periodic, quasiperiodic, and chaotic behaviors. Since these models are essentially autonomous oscillators, they continue to deliver a signal if the action of $E(t)$ ceases.

Declarations

Author contribution statement

Rodrigue Fatou Fonkou, Dr: Conceived and designed the experiments; Performed the experiments; Analyzed and interpreted the data; Contributed reagents, materials, analysis tools or data; Wrote the paper. Patrick Louodop, Associate Professor: Conceived and designed the experiments; Analyzed and interpreted the data; Contributed reagents, materials, analysis tools or data; Wrote the paper. Pierre Kisito Talla, Professor; Paul Wofo, Professor: Conceived and designed the experiments; Analyzed and interpreted the data; Contributed reagents, materials, analysis tools or data.

Funding statement

This research did not receive any specific grant from funding agencies in the public, commercial, or not-for-profit sectors.

Data availability statement

No data was used for the research described in the article.

Declaration of interests statement

The authors declare no conflict of interest.

Additional information

No additional information is available for this paper.

References

- Ahmed, S.H. Javed, S. Abbas, S.K. Hussain, S., Modified van der pol (Vdp) oscillator based cardiac pacemakers, *IEEE Xplore*: 23 February (2017).
 Alhasnawi, Bilal Najj, Jasim, Basil H., Rahman, Zain-Aldeen S.A., Siano, Pierluigi, 2021. A novel robust smart energy management and demand reduction for smart homes based on Internet of energy. *Sensors* 21 (14), 4756.

- Balachandran, V., Kandiban, G., 2009. Experimental and numerical realization of higher order autonomous Van der Pol-Duffing oscillator. *Indian J. Pure Appl. Phys.* 47, 823–827.
 Bao, B.C., Wu, P.Y., Bao, H., Xu, Q., Chen, M., 2018. Numerical and experimental confirmations of quasi-periodic behavior and chaotic bursting in third-order autonomous memristive oscillator. *Chaos Solitons Fractals* 106, 161–170.
 Bendixson, I., 1901. Sur les courbes définies par des équations différentielles. *Acta Math.* 24, 1–88.
 Chaté, H., 1994. Spatiotemporal intermittency regimes of the one-dimensional complex Ginzburg-Landau equation. *Nonlinearity* 7, 185.
 Chedjou, J.C., Fotsin, H.B., Wofo, P., 1997. Behavior of the Van der Pol oscillator with two external periodic forces. *Phys. Scr.* 55, 390.
 Cheng, J., Zhan, Y., 2020. Nonstationary $l_2 - l_\infty$ filtering for Markov switching repeated scalar nonlinear systems with randomly occurring nonlinearities. *Appl. Math. Comput.* 365, 124714.
 Dashkovskiy, S., Pavlichkov, S., 2020. Stability conditions for infinite networks of nonlinear systems and their application for stabilization. *Automatica* 112, 108643.
 D'Heedene, R.N., 1996. For all real $\bar{x} + \mu \sin \bar{x} + x = 0$, has an infinite number of limit cycles. *Differ. Equ.* 5, 564.
 Enrique, L., Gonzalez, B., Bermudez, R.Q., Torres, R.Q., 2020. *Circuits Syst. Signal Process.* 39, 4775–4791.
 FitzHugh, R., 1961. Impulses and physiological states in theoretical models of nerve membrane. *Biophys. J.* 1 (6), 445–466.
 Fonkou, R.F., Louodop, Patrick, Talla, P.K., 2021a. Nonlinear oscillators with state variable damping and elastic coefficients. *Pramana J. Phys.* 95, 210.
 Fonkou, R.F., Louodop, Patrick, Talla, P.K., Wofo, P., 2021b. Van der Pol equation with sine nonlinearity: dynamical behavior and real time control to a target trajectory. *Phys. Scr.* 96, 125203.
 Fonkou, R.F., Louodop, Patrick, Talla, P.K., Wofo, P., 2021c. Dynamic behavior of pacemaker models subjected to a arterial pressure excitation simulator: theoretical and experimental study by microcontroller. *Braz. J. Phys.* 51, 1448–1458.
 Fonkou, R.F., Louodop, Patrick, Talla, P.K., 2022. Dynamical behavior of cardiac conduction system under external disturbances: simulation based on microcontroller technology. *Phys. Scr.* 97, 025001.
 Forger, D.B., 1999. A simpler model of the human circadian pacemaker. *J. Biol. Rhythms* 14 (6), 533–537.
 Grudziński, K., Zebrowski, J.J., 2004. Modeling cardiac pacemakers with relaxation oscillators. *Physica A* 336 (1–2), 153–162.
 Han, X., Zhang, Y., Bi, Q., Kurths, J., 2018. Two novel bursting patterns in the Duffing system with multiple-frequency slow parametric excitations. *Chaos* 28, 043111.
 Han, X.J., Bi, Q.S., 2012. Complex bursting patterns in Van der Pol system with two slowly changing external forcings. *Sci. China, Technol. Sci.* 55, 702–708.
 Han, Y., Xiang, S., Zhang, L., 2019. Cluster synchronization in mutually-coupled semiconductor laser networks with different topologies. *Opt. Commun.* 445, 262–267.
 Hayashi, C., 1964. *Nonlinear Oscillations in Physical Systems*. McGraw-Hill, New York, NY.
 Hochstadt, H., Stephan, B.H., 1967. On the limit cycle of $\ddot{x} + \mu \sin \dot{x} + x = 0$. *Arch. Ration. Mech. Anal.*
 Jasim, B.H., Rashid, M.T., Omran, K.M., 2020. Synchronization and tracking control of a novel 3 dimensional chaotic system. *Iraqi J. Electr. Electron Eng.* 3.
 Joshi, S.K., 2021. Synchronization of coupled oscillators in presence of disturbance and heterogeneity. *Int. J. Dyn. Control* 9, 602–618.

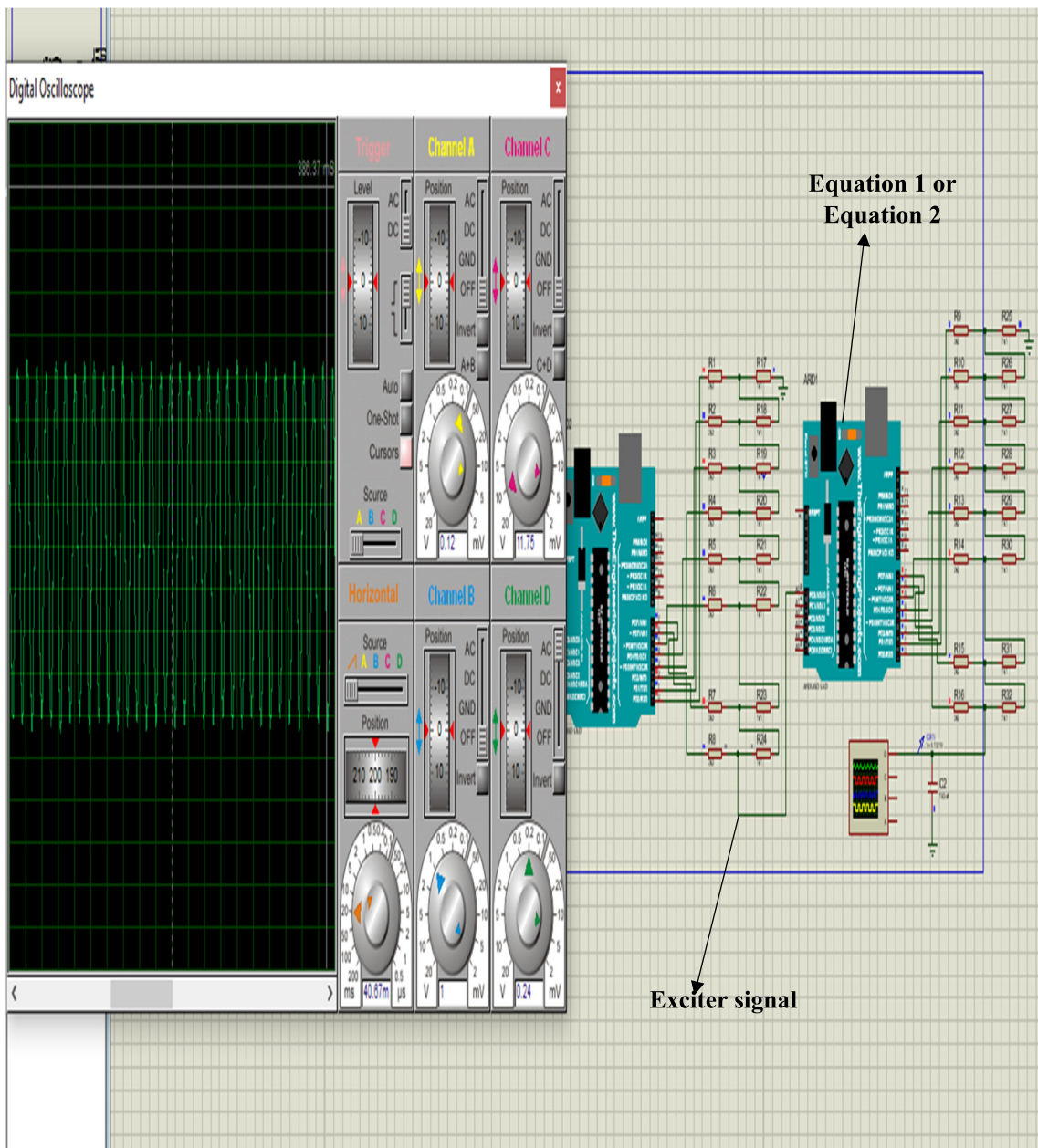


Fig. 17. Microcontroller device representing our exciter signal coupled contains Eq. (1) or Eq. (2).

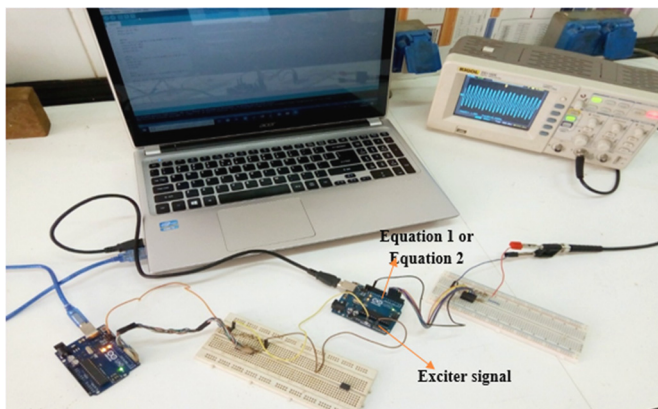


Fig. 18. Experimental device allowing the visualization of the signal.

Kai, T., Tomita, K., 1979. Stroboscopic phase portrait of a forced nonlinear oscillator. *Prog. Theor. Phys.* 61 (1), 54–73.

Kudryashov, Nikolay A., 2018. Exact solutions and integrability of the Duffing - Van der Pol equation. *Regul. Chaotic Dyn.* 23, 471–479.

Lucero, J.C., Schoentgen, J., 2013. Modeling vocal fold asymmetries with coupled van der Pol oscillators. *Proc. Meet. Acoust.* 19, 060165.

Ma, X., Hou, W., Zhang, X., Hand, X., Bi, Q., 2021. A novel bursting oscillation and its transitions in a modified Bonhoeffer-van der Pol oscillator with weak periodic excitation. *Eur. Phys. J. Plus* 136, 998.

Magnitskii, N.A., Sidorov, S.V., 2004. Rotor type singular points of nonautonomous systems of differential equations and their role in the generation of singular attractors of nonlinear autonomous systems. *Differ. Equ.* 40, 1579–1593.

Makouo, L., Wofofo, P., 2017. Experimental observation of bursting patterns in Van der Pol oscillators. *Chaos Solitons Fractals* 94, 95–101.

Rahman, Z., AL-Kashoash, H., Ramadhan, S., Alyasir, Y., 2019. adaptive control synchronization of a novel Menristive chaotic system for secure communication application. *Inventions* 10, 1–11.

Rahman, Zain-Aldeen S.A., Hani Jasim, Basil, Al-Yasir, Yasir I.A., 2021b. New fractional order chaotic system: analysis, synchronization, and it's application. *Iraqi J. Electr. Electron. Eng.* 17 (1).

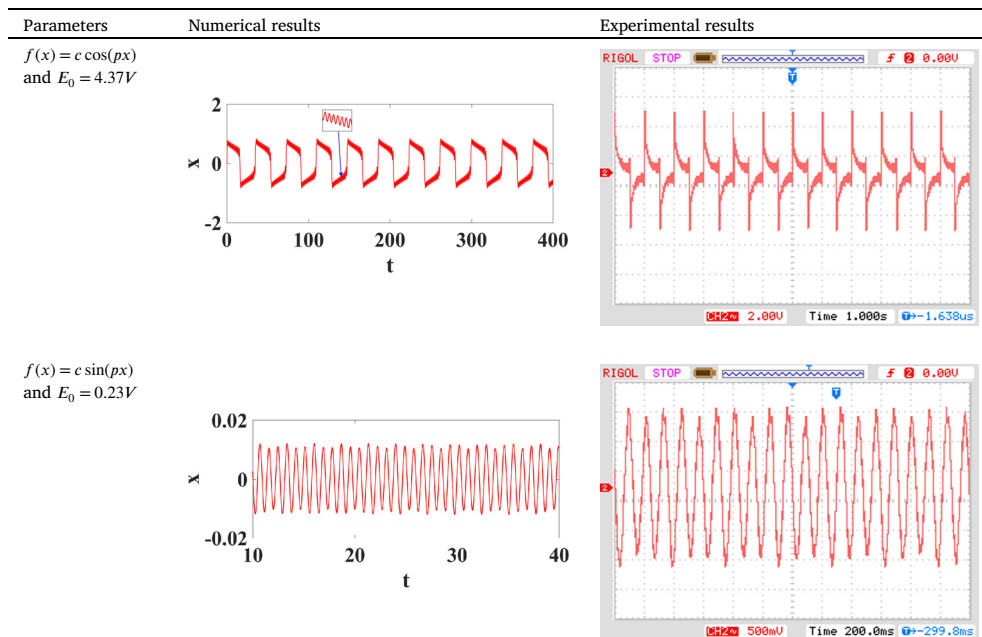


Fig. 19. Chaotic dynamics obtained numerically and by microcontroller, with $x(0) = 0.01$ and $dx/dt(0) = 0.04$.

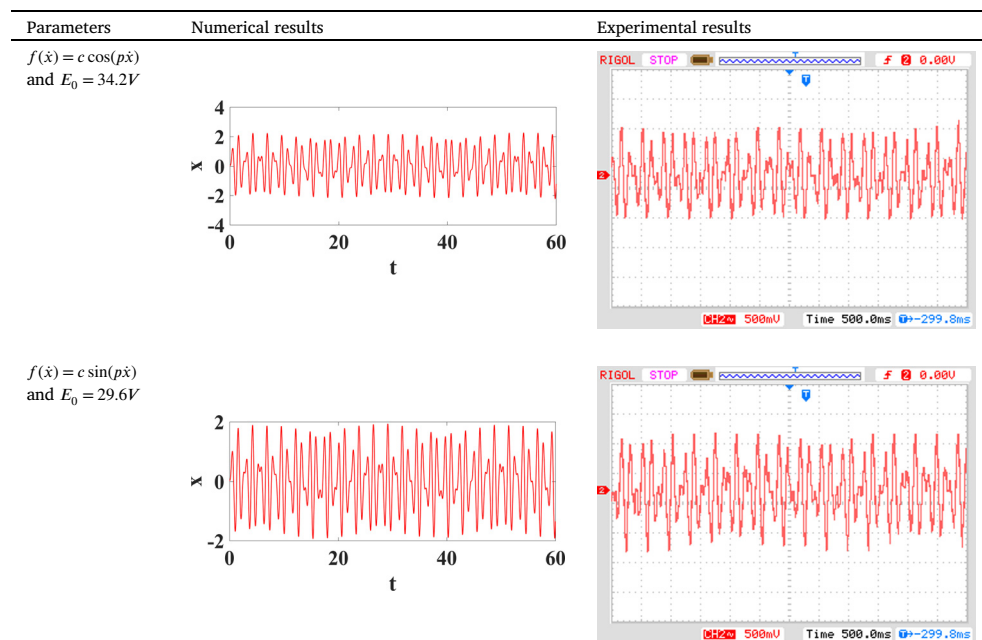


Fig. 20. Chaotic dynamics obtained numerically and by microcontroller, with $x(0) = 0.01$ and $dx/dt(0) = 0.04$.

Rahman, Zain-Aldeen S.A., Jasim, Basil H., Al-Yasir, Yasir I.A., Abd-Alhameed, Raed A., 2021a. High-security image encryption based on a novel simple fractional-order memristive chaotic system with a single unstable equilibrium point. *Electronics* 10, 3130.

Rahman, Zain-Aldeen S.A., Jasim, Basil H., Al-Yasir, Yasir I.A., Abd-Alhameed, Raed A., Alhasnawi, Bilal Naji, 2021c. A new no equilibrium fractional order chaotic system, dynamical investigation, synchronization, and its digital implementation. *Inventions* 6 (3), 49.

Rahman, Zain-Aldeen S.A., Jasim, Basil H., Al-Yasir, Yasir I.A., Hu, Yim-Fun, Abd-Alhameed, Raed A., Alhasnawi, Bilal Naji, 2021d. A new fractional-order chaotic system with its analysis, synchronization, and circuit realization for secure communication applications. *Mathematics* 9 (20), 2593.

Ramirez, J.P., Garcia, E., Alvarez, J., 2020. Master-slave synchronization via dynamic control. *Commun. Nonlinear Sci. Numer. Simul.* 80, 104977.

Rowat, P.F., Selverston, A.I., 1993. Modeling the gastric mill central pattern generator of the lobster with a relaxation-oscillator network. *J. Neurophysiol.* 70 (3), 1030–1053.

Simo, H., Woafu, P., 2012. Bifurcation structure of a Van der Pol oscillator subjected to nonsinusoidal periodic excitation. *Int. J. Bifurc. Chaos* 22 (1), 1250003.

Steeb, W.H., 1977. Nonlinear autonomous dynamic systems, limit cycles, and one-parameter groups of transformations. *Lett. Math. Phys.* 2, 171–174.

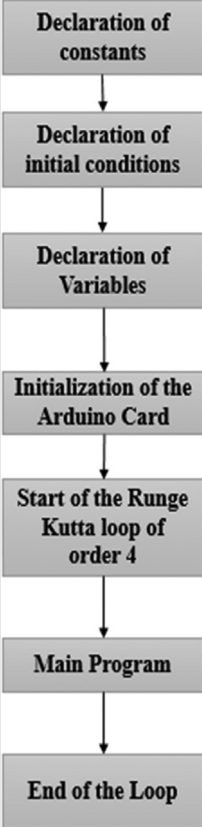
Steeb, W.H., Kunick, A., 1982. Limit cycle oscillations and a perturbed harmonic oscillator. *Int. J. Non-Linear Mech.* 17 (1), 41–45.

Steeb, W.H., Kunick, A., 1983. Painleve property of anharmonic systems with an external periodic field. *Phys. Lett.* 95 (6), 269–272.

Steeb, W.H., Kunick, A., 1987. Chaos in limit cycle systems with external periodic excitations. *Int. J. Non-Linear Mech.* 22 (5), 349–361.

Steeb, W.H., Erig, W., Kunick, A., 1983. Chaotic behaviour and limit cycle behaviour of anharmonic systems with periodic external perturbations. *Phys. Lett. A* 93, 267–270.

Table 2. The Arduino code and the complete flowchart for programming the self-excited oscillator.

The Arduino code	The complete flowchart
<pre> //constants float h=(float)0.1; float a=(float)0.5; float b=(float)0.25; float c=(float)8.; float p=(float)5.0; //initial conditions float x1 =(float)0.01; float y1 =(float)0.04; float t1 =(float)0.0; // vriables double atan(double t1); double sin(double t1); double cos(double t1); float x,x2,y2,t,d; float y,z,r,tt1,xx1; float L1,L2,L3,L4; float M1,M2,M3,M4; void setup() { pinMode (0, OUTPUT); pinMode (1, OUTPUT); pinMode (2, OUTPUT); pinMode (3, OUTPUT); pinMode (4, OUTPUT); pinMode (5, OUTPUT); pinMode (6, OUTPUT); pinMode (7, OUTPUT); pinMode (A0, INPUT); } void loop() { L1=y1; M1=-(-a-c*cos(p*x1))*y1-b*x1; z=x1+(h/2)*L1; r=y1+(h/2)*M1; t=t1+(h/2); L2=r; M2=-(-a-c*cos(p*z))*r-b*z; z=x1+(h/2)*L2; r=y1+(h/2)*M2; t=t1+(h/2); L3=r; M3=-(-a-c*cos(p*z))*r-b*z; z=x1+h*L3; r=y1+h*M3; t=t1+h; L4=r; M4=-(-a-c*cos(p*z))*r-b*z; x1=x1+(h/6)*(L1+2*L2+2*L3+L4); y1=y1+(h/6)*(M1+2*M2+2*M3+M4); t1=t1+h; PORTD=(x1+20)*55.5; x1 = x1; y1 = y1; t1 = t1; } </pre>	 <pre> graph TD A[Declaration of constants] --> B[Declaration of initial conditions] B --> C[Declaration of Variables] C --> D[Initialization of the Arduino Card] D --> E[Start of the Runge Kutta loop of order 4] E --> F[Main Program] F --> G[End of the Loop] </pre>

Tang, Y., Wu, X., Shi, P., Qian, F., 2020. Input-to-state stability for nonlinear systems with stochastic impulses. *Automatica* 113, 108766.

Van der Pol, B., Van der Mark, J., 1926. On "relaxation-oscillations". *Philos. Mag. J. Sci. Ser. 7 2* (11), 978–992.

Van der Pol, B., Van der Mark, J., 1928. The heartbeat considered as a relaxation oscillation, and an electrical model of the heart. *Philos. Mag. J. Sci. Ser. 6*, 763–775.